Rechargeable sodium-ion battery based on a cathode of copper hexacyanoferrate

Rechargeable sodium-ion battery based on a cathode of copper hexacyanoferrate.

Víctor Rojas[1], Gustavo Cáceres[2], Silvana López[2], Rodrigo Henríquez[2], Paula Grez[2], Ricardo Schrebler[2], Emilio Navarrete[3], Francisco Herrera[4], Álvaro Caballero[5], Juan Luis Gómez[5,a], Juliet Aristizábal[6], Eduardo Muñoz[1*].

[1] *Sustrend Laboratorios Spa, Avenida Tupungato 3580, Curauma, Valparaiso*

[2]*Pontificia Universidad Católica de Valparaíso, Instituto de Química, Facultad de Ciencias, Av. Universidad 330, Valparaíso, Chile.*

[3]*Universidad de La Frontera, Departamento de Ciencias Químicas y Recursos Naturales, Facultad de Ingeniería y Ciencias. Av. Francisco Salazar 01145, Temuco, Chile.*

[4]*Universidad de Santiago de Chile, Departamento de Química de los Materiales, Facultad de Química y Biología, Av. Libertador Bernardo O'higgins 3363 Estación Central, Santiago, Chile.*

[5]*Universidad de Córdoba, Departamento Química Inorgánica, Instituto Universitario de Investigación en Química Fina y Nanoquímica, Campus de Rabanales, Universidad de Córdoba, España.*

[6]*Universidad Técnica Federico Santa María, Departamento de Física, Av. España 1680. Valparaíso, Chile.*

[1*] Corresponding author, eduardo.munoz.c@pucv.cl
[a] ISE member.

Abstract.

In this work, the performance of copper(II) hexacyanoferrate(III) (CuHCF) as a cathode material for sodium-ion batteries was studied. The compound was synthesized by a precipitation reaction in aqueous solution in a closed system. The morphology and structure show nanoparticles agglomerated with sizes ranging between 40 and 70 nm and a crystalline phase with a cubic structure, respectively. The material exhibited a stable performance with a working potential of around 3.4 V vs. Na^+/Na. The gravimetric capacity obtained is close to 30 mAh g^{-1} for 100 cycles at a rate of C/20, which is around half of the capacity for CuHCF when it encounters water in its structure, e. g., zeolite-type (60 mAh g^{-1}), which is less than the theoretical capacity for this material (85.1 mAh g^{-1}). CuHCF could be a promising cathode material for sodium-ion batteries considering its electrochemical performance.

Introduction.

Although lithium-ion batteries (LIBs) provide an important solution to implementing sustainable energy and technological development, the feasibility of this element must be reconsidered. Lithium is widely distributed over the earth's crust, but it is not considered an abundant element, being limited to only 20 ppm by mass fraction. Unlike lithium, sodium resources are unlimited, and it is one of the most abundant elements on the planet. Also, sodium is the second lightest and alkali metal with smallest radius after lithium **[1]**. Another advantage to consider is the various economic factors that favor the low cost involved in the manufacturing process of a sodium-ion battery. One of them is that the cathode and electrolyte are composed of Na-based materials, which are cheap **[2]**. In addition, aluminum can be used as a current collector both at the anode and at the cathode, since aluminum undergoes an alloy reaction with lithium below 0.1 V against Li+/Li, a reaction that does not occur for sodium, which indicates that aluminum is available as a current collector for anodes in sodium-ion batteries, leading to a considerable reduction in production costs. Sodium-ion batteries (SIBs) consist of sodium insert materials with an aprotic solvent as the electrolyte. They are therefore free of metallic sodium unless unfavorable reactions (e. g., overcharging) cause the batteries to fail. The structures, components, systems, and charge storage mechanisms are essentially the same as in the LIBs **[1]**. However, there are some differences between these systems. Na^+ ions (1.02 Å) are larger than Li^+ ions (0.76 Å), which affects phase stability, transport properties, and interphase formation. Sodium is also heavier than lithium (23 g mol^{-1} compared to 6.9 g mol^{-1}) and has a slightly less negative standard electrode potential (2.71 V vs. SHE compared to 3.05 V vs. SHE for lithium); and lower gravimetric capacities (1165 mAh g^{-1}, compared to lithium, 3850 mAh g^{-1}) so SIBs will always fall short in terms of its energy density **[3]**. However, despite the difficulties

mentioned above, SIBs have superior technological feasibility since these batteries have the advantage of operating in an aqueous medium **[4]**. Regarding the cathode materials, sodium's insertion/intercalation chemistry is very similar to that of lithium, which allows the same compounds to be used for both systems. Most cathode materials can be classified into two main groups: layered metal oxides or polyanion compounds. These materials reversibly intercalate Na^+ during electrochemical charge/discharge and exhibit stable phase transformations **[5]**. Within them, the compounds known as metal polycyanometalates have been of growing interest as host materials for ions and have been used in rechargeable batteries. Though these compounds present some disadvantages, e. g., high molar mass and low cell voltage, their morphology can be controlled from the synthesis route, structural stability, and they have an excellent retention capacity. From the point of view of hexacyanoferrates with two active metal centers, Yang et al. **[6]** reported the scalable synthesis of single crystals of $Fe^{III}[Fe^{II}(CN)_6]$ (Prussian blue, PB) to reduce structural imperfections obtaining near-perfect morphology. The material delivered a reversible capacity of 120 mAh g^{-1} at 0.5 C, with 87% retention capacity over 500 cycles, showing great promise for SIBs applications. These results provided insight into PB analogs' intercalation/insertion chemistry and opened new perspectives to develop Na^+ storage cathodes for widespread electrical energy storage applications **[7, 8, 9, 10]**. Regarding hexacyanoferrates with one electroactive metal center, You et al. **[11]** synthesized nickel hexacyanoferrate (NiHCF) with zero strain for sodium-ion batteries, using a wet chemical method. NiHCF exhibits capacities close to 60 mAh g^{-1} and excellent cyclic stability with a 99.7% retention capacity for 200 cycles and a high coulombic efficiency of close to 100%. Considering the excellent cyclic and structural stability, a simple synthesis procedure, and the low cost for the precursors these Prussian blue analogs are interesting for their use in

sodium-ion batteries. Copper hexacyanoferrate (CuHCF) has been recently studied which presents a simple synthesis route, particles around nanometric sizes, good electrochemical reversibility, and a cubic-type crystalline structure that allows a wide variety of ions insertion, e. g., alkalines, mono, and polyvalent. The general formula for these materials is $A_xPR(CN)_6$, and their crystal structure is analogous to that of the ABX_3 perovskites, with P^{m+} and R^{n+} ions in an ordered arrangement on the B sites. The occupancy of the tetrahedrally coordinated A sites in the large cages in this crystallographically porous framework may vary from x=0 to x=2, with corresponding changes in the valence of one or more of the P and R species **[12]**. This study aimed to evaluate the electrochemical insertion of sodium ions through the analysis of charge/discharge curves in a button cell battery. In this work, copper hexacyanoferrate (CuHCF) nanoparticles were hydrothermally obtained, characterized by different techniques, and employed as a cathode in SIBs. It was possible to study satisfactorily, obtaining capacities close to 30 mAhg-1, high cyclic stability, and efficiencies close to 95% during 100 cycles.

Experimental.

Synthesis and purification of CuHCF.

CuHCF were synthesized hydrothermally by using 0.125 M $K_3[Fe(CN)_6]$ and 0.25 M $CuCl_2 \cdot 2H_2O$ as precursors of $[Fe(CN)_6]^{-3}$ and Cu^{+2}, respectively, and 1 M KCl as the charge of potassium to the compound. 20 mL of each solution were mixed in a 100 mL beaker with constant stirring for 10 minutes. At the end of this time, the mixture was transferred to a Teflon cell contained in a stainless-steel autoclave reactor were kept for 2 hours at a constant temperature of 30ºC. After the reaction, the reactor was cooled to room temperature, obtaining a colloidal solution centrifuged at 4500 rpm to separate the solid from the supernatant. The product CuHCF was washed three times with deionized water and allowed to dry in an oven at 60°C.

Material characterization:

The powder obtained was characterized by X-ray diffraction (XRD, Bruker model D8 Advance with Cu tube (40 mA, 40 kV)), field emission scanning electron microscopy (FESEM, QUANTA FEG250), transmission microscopy electronics (TEM, JEOL JEM 1400) and thermogravimetric analysis (TGA / DSC 1 Star System, Mettler Toledo) using a N_2 flow of 100 mL min^{-1} with a temperature ramp from 25 - 700 ° C.

Electrode preparation:

To prepare the electrode material, first the CuHCF was washed with deionized water and dried under vacuum at 100 ° C for 12 hours to remove the remaining KCl from the synthesis. Then, CuHCF was mixed with super P carbon (Timcal) and polyvinylidene difluoride (PVDF, Aldrich) in proportions of 80:10:10, respectively, in N-Methyl-2 -Pyrrolidone (NMP, ITW reagents) as dispersing agent for 30 minutes at 4000 rpm using an Ultra-Turrax disperser (IKA digital model T18). The resulting suspension was deposited on a carbon

current-collector (GDL ELAT1400, Fuel Cells Store) using the Dr. Blade technique. Finally, the composite deposited on the carbon substrate was dried at 50° C for 12 hours in an oven to evaporate the solvent completely. The electrodes were cut in circles with a diameter of 13 mm (deposited mass 7 mg cm^{-2}) and vacuum-dried at a temperature of 100°C for 3 hours using a glass vacuum oven (Buchi). After drying, the electrodes were transferred to a MBraun 150 glove chamber with controlled argon atmosphere for mounting coin-type batteries (CR2032).

Electrolyte preparation:

An electrolyte of 1M $NaPF_6$ (Aldrich) in propylene carbonate (PC, Aldrich) was prepared. The $NaPF_6$ salt was dried for 72 hours at 110 °C in a glass oven (Buchi). The PC solvent was passed three times through zeolite previously dried at 200°C for 72 hours to extract moisture from the solvent. Finally, 10 mL of 1M $NaPF_6$ electrolyte was prepared in an MBraun 150 glove chamber.

Sodium batteries assembly:

The configuration used in electrochemistry measurements was a half-cell where the negative electrode was a metal sodium chip with a diameter of 13 mm, a Whatman filter of 16 mm diameter fiberglass was used as a separator, and 1 M $NaPF_6$ electrolyte in a propylene carbonate, wich was previously prepared. Finally, the battery was hermetically sealed using a hydraulic press, applying a pressure of 800 psi.

Electrochemical measurements:

Cyclic voltammetry (CV) measurements were performed using a potenciostat/galvanostat (Autolab, PGSTAT204) in the potential range of 2.5 – 4.3 V vs Na^+/Na. Galvanostatic charge/discharge cycling tests of the cells were performed in a voltage of 2.5 – 4.3 V vs

Na^+/Na in a battery tester Arbin BT2143. The program employed started in discharge mode from open-circuit voltage (3.1 V vs. Na^+/Na) until 2.5 V, and later was charged until 4.3 V.

Results and discussions.

XRD characterization.

The crystal structure and phase of the material was determined by powder X-ray diffraction shown in Figure 1(a). The synthesized CuHCF powders show a high crystallinity and the diffraction peaks can be indexed in the face centered cubic structure of $Cu(Fe(CN)_6)_{0.667}$ (86-0513; $Fm\bar{3}m$, $a = b = c = 10.1$ Å). The reaction that summarizes the formation of CuHCF can be represented as:

$$K_3Fe(CN)_{6(aq)} + CuCl_{2(aq)} + (n+1)H_2O_{(l)} \rightarrow KCu[Fe(CN)_6] \times nH_2O_{(s)} + 2KCl_{(aq)} + H_2O_{(l)} \quad (1)$$

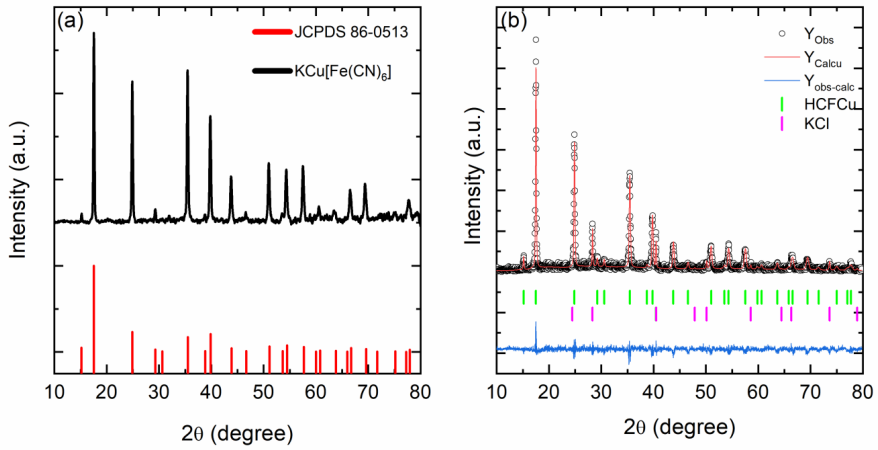

Figure 1: (a) XRD patterns of $KCu[Fe(CN)_6]$ nanoparticles obtained and (b) Rietveld refined powder XRD pattern of the as-synthesized $KCu[Fe(CN)_6]$.

Crystallite size was estimated by Rietveld analysis using the XRD peak indexing software FULLPROF, as shown in Figure 1(b). This information was used to identify the unit cell

lattice symmetry cubic belonging the $Fm\bar{3}m$ space group (CIF Code 1010359), with the unit cell parameters determined to be as follows: $a = b = c = 10.121(4)$ Å, $\alpha = \beta = \gamma = 90°$ and crystal size 67 nm. The R parameters were $R_p = 20.0$, $R_{wp} = 29.4$, $R_{exp} = 35.5$ and $\chi^2 = 1.54$. The CuHCF, whose structure was proposed by Keggin and Miles **[13]**, it consists of a simple cubic with chains of –Fe−C−N−Cu−N−C−Fe− along the three crystallographic directions forming an octahedron. Each unit cell consists of eight cells and therefore contains eight insert sites that allow both monovalent and polyvalent ions to be accommodated. Cell size is an important parameter to facilitate insertion of sodium-ion (95 pm), in this case (10.121 Å = 1012 pm), therefore it is possible to house these ions.

Characterization by FESEM, TEM and TGA.

Field emission scanning electron microscopy (FESEM) was used to study the morphology of the CuHCF. The FESEM images shown in Figure 2(a), indicate a particle size ranged between 40 and 70 nm corresponding to usual morphologies of these agglomerates, and consistent with those determined by XRD. Using transmission electron microscopy (TEM, Fig. 2b), it can be seen that the particles are agglomerated and with a cubic morphology that cannot be appreciated by FESEM. Analogs of PB compounds generally have water in their structure, which can be found in two forms: a) as zeolitic H_2O in the cavities formed by the M'−CN−M network, and b) as coordinated H_2O replacing vacancies of the octahedron cavities formed by $Fe(CN)_6^{3-}$ **[14, 15]**. According to the XRD analysis, the synthesized CuHCF has a vacancy fraction of 0.6. The TGA in Figure 2(c) shows that weight loss occurs in two steps.

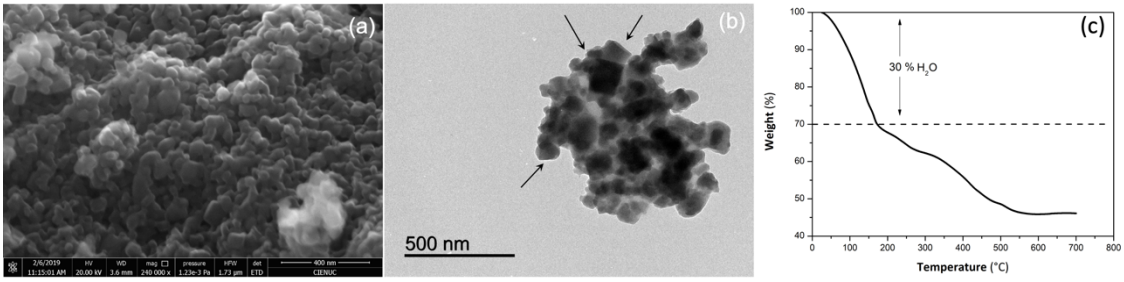

Figure 2: a) FESEM image; b) TEM image and; c) TGA curve of prepared CuHCF nanoparticles.

According to Figure 2(c), heating from room temperature to about 180° C, produces 30% of mass loss corresponding to: i) adsorbed humidity, zeolitic water and coordinated water in the structure, i. e., equivalent to 6 molecules per unit of formula. Above 180° C, a gradual decomposition of the CN group into $(CN)_2$ occurs, obtaining Cu and Fe as final products **[16]**. Therefore, the molecular formula of the synthesized compound can be considered to have now six more water molecules, $KCu[Fe(CN)_6]_{0.667}\cdot 6H_2O$.

Electrochemical performance of CuHCF as a cathode for SIBs.

The electrochemical performance of the cathode was evaluated using CV and galvanostatic charge-discharge curves (GC) at room temperature, under the experimental conditions described in the experimental section. Figure 3 shows a quasi-reversible insertion (3.3 V) and extraction (3.7 V) process of sodium ions, with a peak-potential separation around 400 mV and a ratio of oxidation/reduction areas close to 1. These redox reactions correspond to iron (Fe^{2+} / Fe^{3+}) coordinated to the carbon atom in the HCFCu structure. The following equation can represent the process of insertion of sodium ions during iron reduction:

$$KCu^{(II)}[Fe^{(III)}(CN)_6]\cdot nH_2O + xNa^+ + xe^- \leftrightarrow Na_xKCu^{(II)}[Fe^{(II)}(CN)_6]_x[Fe^{(III)}(CN)_6]_{1-x}\cdot nH_2O \quad (2)$$

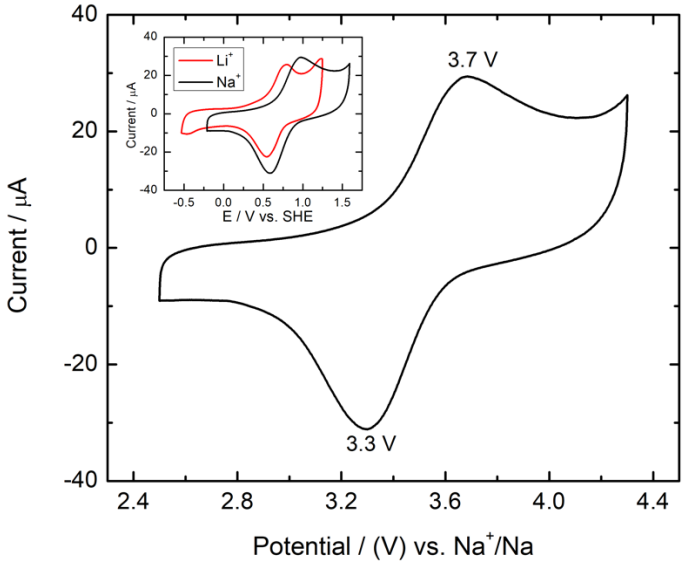

Figure 3: CV of a sodium half-cell with CuHCF as cathode at a scan rate of 0.1 mV s^{-1} in a potential range of 2.5 - 4.3 V vs. Na^+/Na. (inset) CV for CuHCF as a cathode in lithium and sodium half-cells at a scan rate of 0.1 mV s^{-1} vs. the standard hydrogen electrode (S.H.E.). Electrolyte composition: 1 M $NaPF_6$ in propylen carbonate for sodium cell. 1 M of $LiPF_6$ in Ethylen:Diethylencarbonate (EC:DEC; 50:50) for lithium cell.

The reduction/oxidation potential depends on the cation inserted into the HCFCu structure. Let us compare the potentials versus the standard hydrogen electrode (S.H.E., Figure 3). The reduction potential of CuHCF is 0.55 V and 0.59 V in lithium and sodium electrolytes, respectively, related to the different energies for ion desolvation in these media. Additionally, the oxidation potential is 0.59 V and 0.99 V in lithium and sodium, respectively, indicating smaller cations are favored to exit from the lattice.

The C-Rate study (Figure 4a) shows the highest capacities at a charge/discharge rate of C/20, obtaining values close to 30 mAh g^{-1}. Figure 4b shows the galvanostatic profile at different charge-discharge rates, obtaining much more defined plateaus at low-rate at potentials close to 3.3 V and 3.7 V for discharge and charge, respectively, the same results found through cyclic voltammetry measurements. Finally, the Ragone plot for CuHCF is shown in Figure 4(c). Specific energy around 25 W h/kg and 85 W h/kg were reached when the system was discharged at 1C and C/20, respectively. Additionally, a specific power of around 7 mW/kg and 1.5 W/kg are achieved at discharge rates of 1C and C/20, respectively.

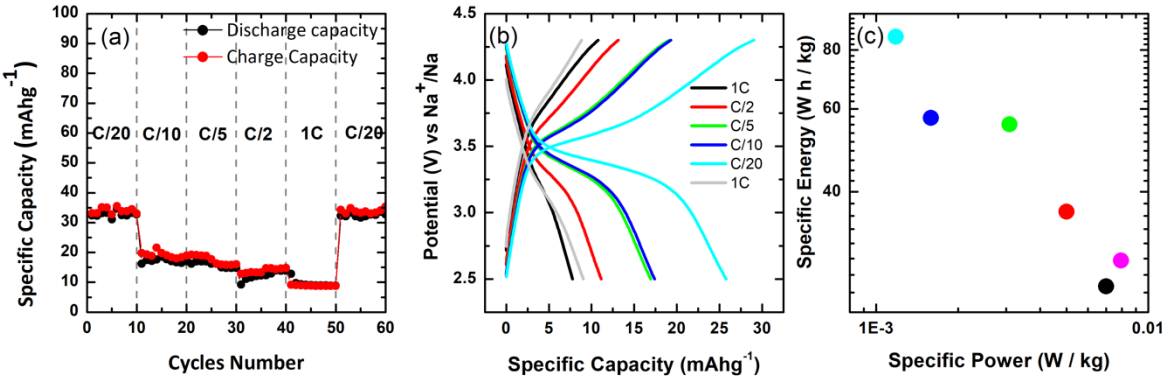

Figure 4: a) Specific capacity as a function of the cycles number; b) galvanostatic charge/discharge profiles of CuHCF at different current densities (C-Rate study), and c) the Ragone plot for CuHCF.

The galvanostatic profile in Figure 4b shows only a plateau for both charge and discharge. When sodium ions are inserted, Fe^{3+} is reduced to Fe^{2+} at 3.3 V. Afterwards, Fe^{2+} is oxidized to Fe^{3+} at 3.7 V in the extraction process. As for lithium, the charging process is facilitated considering the absence of a hydration sphere during the extraction process, which is associated with a significant charge capacity compared to the discharge capacity. For C/20,

the charging process reaches values close to 30 mAh g^{-1}, while for the discharge this value decreases reaching values close to 26 mAh g^{-1}.

The average specific capacity and retention capacity for CuHCF obtained in this study are summarized in Table I. The results show a decrease in the retention of the initial capacity as the rate of the charge/discharge process increases, showing the influence of the diffusion rate of Na^+ ions inside the CuHCF structure. The initial capacity is reached to retain 96.4% for C/20, between the initial and final cycles, therefore, a rate C/20 has been chosen to carry out the galvanostatic cyclability studies.

Table I: Average discharge specific capacity (mAh g^{-1}) and retention capacity (%) at different charge/discharge rates (C) for the CuHCF.

	$C/20_{init}$	C/10	C/5	C/2	1C	$C/20_{final}$
Discharge specific capacity (mAh g^{-1})	25.1	17.2	15.9	12.3	8.10	24.2
Retention capacity (%)	100	68.5	63.3	49.0	32.3	96.4

Figure 5a shows the charge/discharge profiles, which have been divided into different zones. In discharge mode (down arrows), it can be seen three zones: (I), (II), and (III). In zone (I), from the upper cut-off potential (app. 4.3 V) to about 3.5 V, the potential drops sharply due to cell polarization. These conditions increase the internal cell impedance (ohmic resistance) and the compound's solubility. Subsequently, a pseudo plateau is produced in the zone (II) between 3.5 V to 3.2 V. The composition range of this zone is around $0.1 < x < 0.3$, typical of a topotactic transition described by Equation (2). Here, sodium ions insert into the CuHCF structure, occupying the octahedron's sites. During this insertion, Fe^{3+} is reduced to Fe^{2+} at a

potential close to 3.3 V. In zone (III), a single-phase reaction with its abrupt drop in potential occurs again (lowest cut-off potential, approximately 2.5 V). According to these results, the insertion of sodium ions reaches a maximum of x = 0.44 during the first discharge cycle and an average of x = 0.40, considering the first 50 cycles and a final value of x = 0.38 for cycle 100. In the charging mode (up arrows), three zones can be observed: (i), (ii), and (iii). In zone (i), there is a significant potential increase from 2.5 V to 3.4 V, with the removal of sodium ions around x = 0.05. Subsequently, in zone (ii), a pseudo plateau is observed between 3.4 V and 3.7 V associated with the oxidation of Fe^{2+} to Fe^{3+} at this potential with the removal of x = 0.30 (cycle 50) and x = 0.2 (cycle 100) of sodium ions. These results show the stability of the coulombic efficiency associated with the high retention capacity at C/20. A graph of the remaining capacity percentage as a function of the cycle numbers indicates a capacity of 99.7% in the tenth cycle. However, when cycling increases, the remaining available capacity decreases by an average of 97% over nearly 100 cycles. The high remanent capacity and high coulombic efficiency suggest that the host material has excellent reversibility for charge/discharge processes and life cycle.

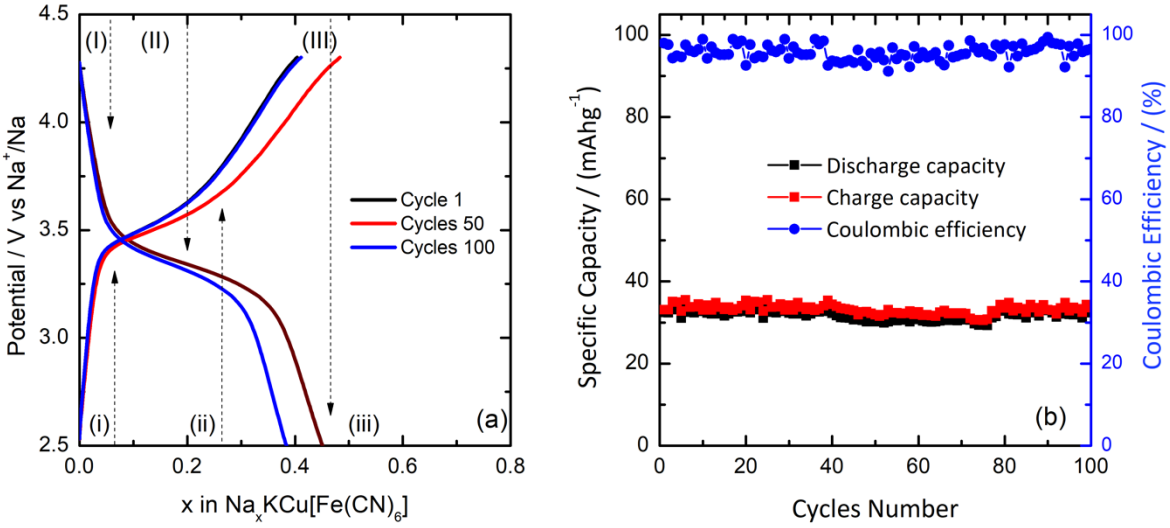

Figure 5: a) Galvanostatic charge/discharge profile at C/20 and; (b) the specific capacity and coulombic efficiency as function of cycle numbers.

Figure 5b shows the results of the specific capacity and coulombic efficiency concerning the number of cycles. During the 100 cycles, a coulombic efficiency of 90% on average is obtained. The higher charge capacity achieved compared to the discharge capacity (because the reduction/discharge process is more difficult due to the larger size of the sodium ion) causes a decrease in the efficiency. The capacities reached by the material are half of the practical capacity of CuHCF ($C_{Theoretical\ anhydrous}$= 85.1 mAh g^{-1}, $C_{Practical}$ = 60 mAh g^{-1}). An additional capacity loss is attributed to the larger size of the sodium ion, presenting more resistance to diffusion in the electrolyte and the compound's structure, inserted with only up to 0.5 sodium ions per formula unit **[17]**. Another critical factor that influences this performance is the presence of moisture in the electrolyte preparation. Because the electrolyte

is prepared and not of commercial origin, the water remotion could present difficulties, leaving water in the PC solvent and promoting the decomposition of $NaPF_6$, which would produce more insulating compounds, as shown in the following equation **[18]**:

$$2NaPF_6 + H_2O \rightarrow Na_2O + 2HF + 2PF_5 \quad (3)$$

Finally, it is important to emphasize the influence of the zeolitic water in the interstitial sites, which compete with the sodium ions in the insertion process. Ideally, zeolitic water should be eliminated due to its adverse effect on sodium. Because of this, it is expected that in later studies, it will be possible to eliminate the structural humidity of the compound to improve its performance. The presence of transition metal vacancies reduces the charge stored when the redox reaction occurs and the zeolitic water molecules occupy the interstitial sites the same as the sodium-ion. Ideally, the coordination water should be retained to ensure the stability of the open crystal structure, while the zeolitic water should be removed due to its adverse effect on the initial sodium content. For example, Song et al. **[19]** reported the effect on the structure and electrochemical properties of sodium manganese(II) hexacyanoferrates(II) after the remotion of interstitial H_2O. The dehydrated phase exhibits superior electrochemical performance compared to other reported Na^+ ion cathode materials, delivering 3.5 V with a reversible capacity of 150 mAh g^{-1} in a sodium half-cell and 140 mAh g^{-1} in a full-cell, using a carbon anode. The material synthesized in the present work presents performance well below those described in the bibliography, projecting improvements in the synthesis process, electrolyte preparation, and battery assembly, avoiding the presence of water in the process. In Table II, a comparison can be seen between the material studied in this work and other types of Prussian blue analogs. Additionally, some classic materials in the study of this type of battery are also included.

Table II: Comparison of the electrochemical performance of HCFCu synthesized in this work regarding other cathode materials in SIBs.

Compound	**Ref.**	**Working potential**	**Synthesis**	**C-rate**	**Specifical Capacity mAh g^{-1}**
CuHCF	*	3.5	Hydrothermal	C/20	30
MnHCF	[20]	3.4	Co-precipitation	C/10	120
NiHCF	[21]	3.4	Co-precipitation	1.1C	90
CoHCF	[22]	3.2	Co-precipitation	0.59C	90
CuHCF	[23]	3.3	Co-precipitation	C/4	40
FeHCF	[24]	3.2	Co-precipitation	2C	120
$Na_{0.7}CoO_2$	[25]	2.3	Solvothermal	C/10	140
NASICON Full Cell	[26]	1.7	Precipitation	10C	90

* This work

The American spin-off Natron Energy (United States) developed a sodium-ion battery using an analog of Prussian blue in both the cathode and the anode, with an aqueous electrolyte. This configuration provides lower energy densities than in an organic electrolyte. However, on the other hand, it allows power density values of 775 W kg^{-1} (or 1550 W/L) at a current intensity of 12C, reaching 25000 cycles. What is more, they have recently developed a commercial Natron's BlueTray™ 4000 battery available for data centers or

telecommunications **[27]**. These data indicate that PBs may well fit into commercial products as alternatives to current lithium-ion batteries.

Conclusions.

This work has allowed us to corroborate that our synthesis methodology, as in previous works, leads us towards the desired product, which is confirmed by the different characterization analyses used. Although our material does not exhibit a high capacity, the electrochemical studies carried out to provide us with knowledge of the behavior of CuHCF in SIBs, but also new research challenges, which are shared by other groups at an international level, given the technological potential that they present the family of polycyanometalates and sodium-ion batteries.

Acknowledgements.

We acknowledge the financial support from FONDECYT, Chile, (grant no. 1210408), from VRIEA-PUCV (grant no. 039.438 NÚCLEO-PUCV and 125.737/22 DII-PUCV), from the Spanish Ministerio de Economía y Competitividad (Project MAT2017–87541-R) and from Junta de Andalucía (Group FQM-175) and from FONDEQUIP EQM150101. E. Navarrete and J. Aristizábal thank for the financial support from postdoctoral project FONDECYT (N° 3200216 and 31210536, respectively). V. Rojas would like to acknowledge the kind support from his doctoral scholarship by ANID N° 21160733. F. Herrera thanks DICYT-USACH for their financial support.

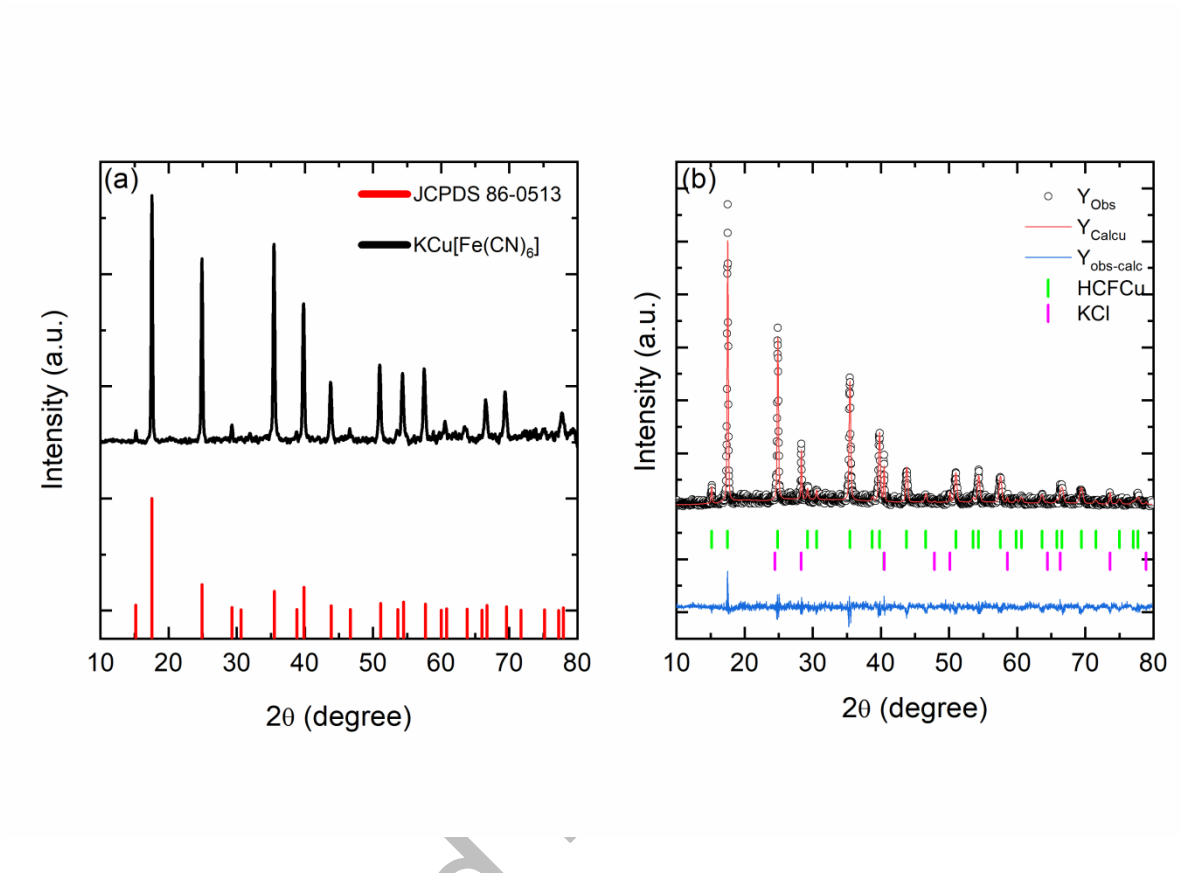
(a)
JCPDS 86-0513
KCu[Fe(CN)6]
Intensity (a.u.)
10 20 30 40 50 60 70 80
2θ (degree)
(b)
Yobs
Ycalcu
Yobs-calc
HCFCu
KCl
Intensity (a.u.)
10 20 30 40 50 60 70 80
2θ (degree)

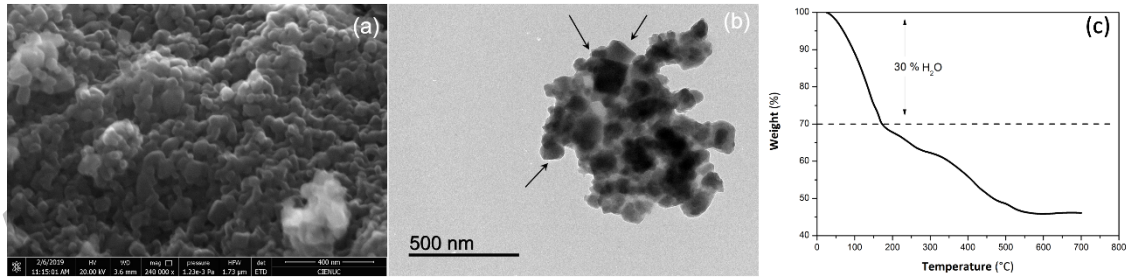
(a)
(b)
500 nm
(c)
30 % H2O
Weight (%)
100 90 80 70 60 50 40
0 100 200 300 400 500 600 700 800
Temperature (°C)

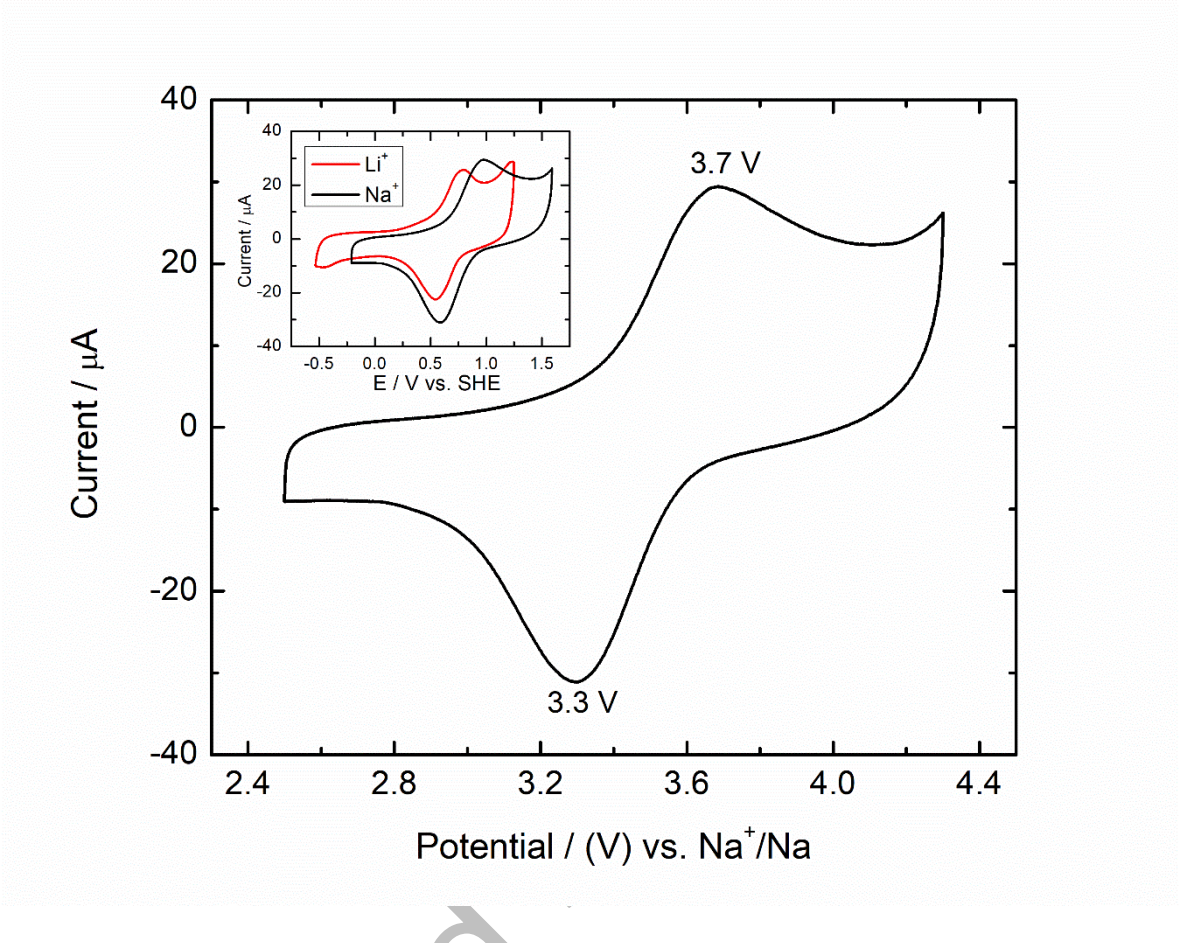
Current / μA
Potential / (V) vs. Na+/Na
3.7 V
3.3 V
Li+
Na+
E / V vs. SHE

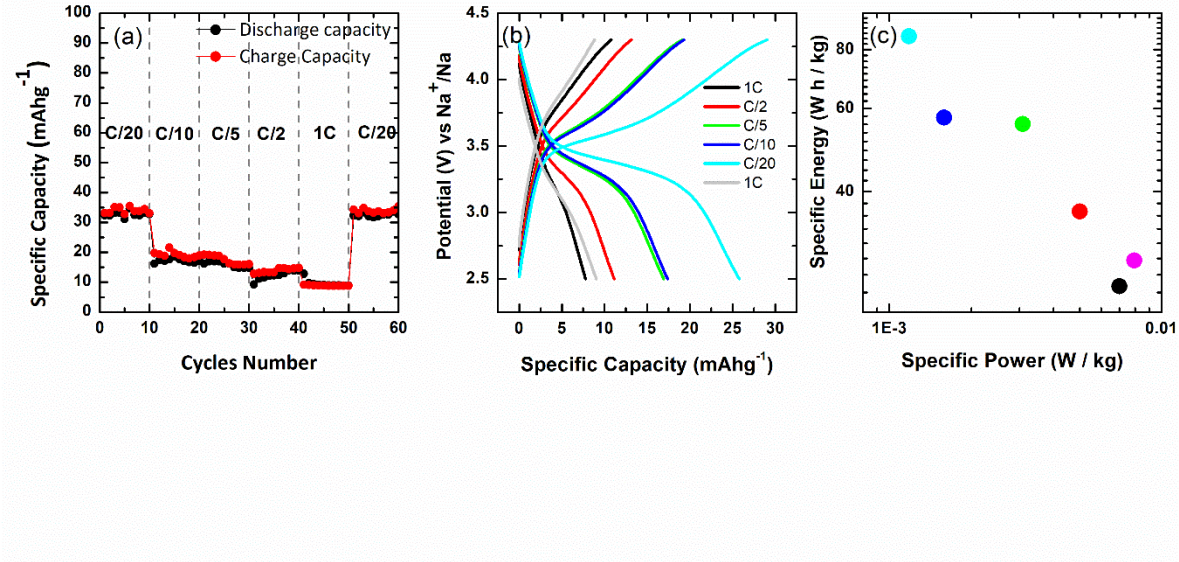
(a)
Discharge capacity
Charge Capacity
C/20
C/10
C/5
C/2
1C
C/20
Specific Capacity (mAhg-1)
Cycles Number
(b)
1C
C/2
C/5
C/10
C/20
1C
Potential (V) vs Na+/Na
Specific Capacity (mAhg-1)
(c)
Specific Energy (W h / kg)
Specific Power (W / kg)

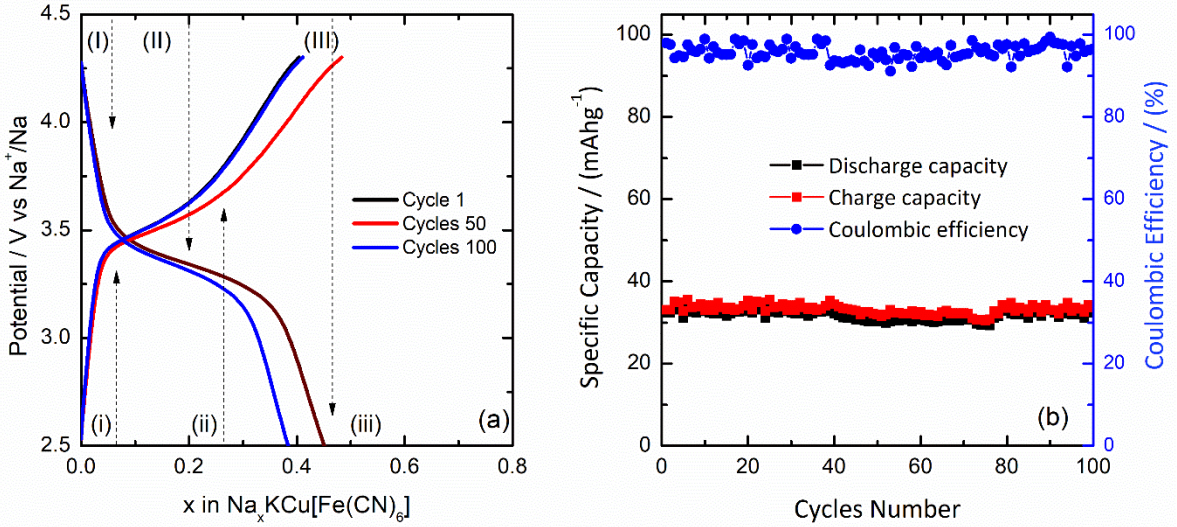

[1] Yabuuchi N, Kubota K, Dahbi M, Komaba S (2014) Research development on sodium-ion batteries. Chem Rev 114:11636-11682.

[2] Perveen T, Siddiq M, Shahzad N, Ihsan R, Ahmad A, Shahzad MI (2020) Prospects in anode materials for sodium ion batteries - A review. Renew Sustain Energy Rev 119:109549.

[3] Hwang JY, Myung ST, Sun YK (2017) Sodium-ion batteries: Present and future. Chem Soc Rev 46:3529.

[4] Guduru RK and Icaza JC (2016) A Brief Review on Multivalent Intercalation Batteries with Aqueous Electrolytes. Nanomaterials **6**:41.

[5] Chayambuka K, Mulder G, Danilov DL, Notten PHL (2018) Sodium-Ion Battery Materials and Electrochemical Properties Reviewed. Adv Energy Mater 8:1800079.

[6] Wu X, Deng W, Qian J, Cao Y, Ai X, Yang H (2013) Single-crystal $FeFe(CN)_6$ nanoparticles: A high capacity and high rate cathode for Na-ion batteries. J Mater Chem A 1:10130.

[7] Wang J, Mi C, Nie P, Dong S, Tang S, Zhang X (2018) Sodium-rich iron hexacyanoferrate with nickel doping as a high performance cathode for aqueous sodium ion batteries. J Electroanal Chem 818:10.

[8] Liu Y, Qiao Y, Zhang W, Li Z, Ji X, Miao L, Yuan L, Hu X, Huang Y (2015) Sodium storage in Na-rich NaxFeFe(CN)6 nanocubes. Nano Energy 12:386.

[9] Wang L, Song J, Qiao R, Wray LA, Hossain MA, Chuang Y, Yang W, Lu Y, Evans D, Lee J, Vail S, Zhao X, Nishijima M, Kakimoto S, Goodenough JB (2015) Rhombohedral Prussian White as Cathode for Rechargeable Sodium-Ion Batteries. J Am Chem Soc 137:2548.

[10] Lim C, Tan Z (2021) Prussian White with Near-Maximum Specific Capacity in Sodium-Ion Batteries. ACS Appl Energy Mater 4:6214.

[11] You Y, Wu XL, Yin YX, Guo YG (2013) A zero-strain insertion cathode material of nickel ferricyanide for sodium-ion batteries. J Mat Chem A 45:14061.

[12] Wessells CD, Huggins RA, Cui Y (2011) Copper hexacyanoferrate battery electrodes with long cycle life and high power. Nat. Commun. 2:550.

[13] Keggin JF, Miles FD (1936) Structure and formule of the Prussian Blues and related compounds. Nature 137:577.

[14] Ojwang DO, Grins J, Wardecki D, Valvo M, Renman V, Häggström L, Ericsson T, Gustafsson T, Mahmoud A, Hermann RP, Svensson G (2016) Structure Characterization and Properties of K-Containing Copper Hexacyanoferrate. Inorg Chem 55:5924.

[15] Hurlbutt K, Wheeler S, Capone I, Pasta M (2018) Prussian Blue Analogs as Battery Materials. Joule 2:1950.

[16] Åkerblom IE, Ojwang DO, Grins J, Svensson G (2017) A thermogravimetric study of thermal dehydration of copper hexacyanoferrate by means of model-free kinetic analysis. J Therm Anal Calorim 129:721.

[17] Wang B, Han Y, Wang X, Bahlawane N, Pan H, Yan M, Jiang Y (2018) Prussian Blue Analogs for Rechargeable Batteries. iScience 3:110.

[18] Zheng LQ, Li SJ, Lin HJ, Miao YY, Zhu L, Zhang ZJ (2014) Effects of water contamination on the electrical properties of 18650 lithium-ion batteries. Russ J Electrochem 50:904.

[19] Song J, Wang L, Lu Y, Liu J, Guo B, Xiao P, Lee J, Yang X, Henkelman G, Goodenough JB (2015) Removal of interstitial H_2O in hexacyanometallates for a superior cathode of a sodium-ion battery. J Am Chem Soc 137:2658.

[20] Wang L, Yuhao L, Liu J, Xu M, Cheng J, Zhang D, Goodenough JB (2013) A superior low-cost cathode for a Na-Ion battery, Angew. Chem. Int. Ed. 52:1964.

[21] Ren W, Qin M, Zhu Z, Yan M, Qi L, Zhang L, Liu D, Mai L (2017) Activation of Sodium Storage Sites in Prussian Blue Analogues via Surface Etching. Nano Lett. 17:4713.

[22] Yuan Y, Wang J, Hu Z, Lei H, Tian D, Jiao S (2016) $Na_2Co_3[Fe(CN)_6]_2$: A promising cathode material for lithium-ion and sodium-ion batteries. J. Alloys Compd. 685:344.

[23] Jiao S, Tuo J, Xie H, Cai Z, Wang S, Zhu J (2017) The electrochemical performance of $Cu_3[Fe(CN)_6]_2$ as a cathode material for sodium-ion batteries. Mat. Res. Bull. 86:194.

[24] Wu X, Deng W, Qian J, Cao Y, Ai X, Yang H (2013) Single-crystal $FeFe(CN)_6$ nanoparticles: A high capacity and high rate cathode for Na-ion batteries. J. Mat. Chem. A 1:10130.

[25] Peng B, Sun Z, Jiao S, Li J, Wang G, Li Y, Jin X, Wang X, Li J, Zhang G (2019) Facile self-templated synthesis of P2-type $Na_{0.7}CoO_2$ microsheets as a long-term cathode for high-energy sodium-ion batteries. J. Mat. Chem. A. 7:13922.

[26] Jiang Y, Zhou X, Li D, Cheng X, Liu F, Yu Y (2018) Highly Reversible Na Storage in $Na_3V_2(PO_4)_3$ by Optimizing Nanostructure and Rational Surface Engineering. Adv. Energy Mater. 8:1800068.

[27] "Home - Natron." https://natron.energy/ (accessed Sep. 24, 2021).